DOI: 10.2478/sbeef-2023-0024

SIMULATED SURFACE ELECTROMYOGRAPHIC (SEMG) SIGNAL GENERATION AND DETECTION MODEL

Noureddine MESSAOUDI[(1), (2)], Samia BELKACEM[(1), (3)], Rais El'hadi BEKKA[(4)]
[(1)] University of Boumerdes, Faculty of Technology, Department Electrical Systems Engineering, 35000 Boumerdes, Algeria
[(2)] University of Boumerdes, Faculty of Technology, LIST Laboratory, 35000 Boumerdes, Algeria
[(3)] University of Boumerdes, Faculty of Sciences, LIMOSE Laboratory, 35000 Boumerdes, Algeria
[(4)] University of Sétif 1, Faculty of Technology, Department of Electronics, LIS Laboratory, 19000 Sétif, Algeria
Email: n.messaoudi@univ-boumerdes.dz

Abstract. ***For didactic purposes, the aim of this work was to improve a simulation model of surface electromyographic (sEMG) signal by taking into consideration the shortcomings of previously developed models. This model started with the simulation of the single fibre action potential (SFAP), then the model of the single motor unit action potential (MUAP), afterwards the imitation of the train of MUAP and finally the modellig of the resultant sEMG signal which is the sum of the MUAPs trains. SFAP simulation was based on: i) the description of the volume conductor model which is composed of four layers (bone, muscle, fat and skin), ii) the description of the electrodes shapes and sizes as well as spatial filters, iii) and the transmebrane current. The proposed model shows its effectiveness in the possibility of carrying out practical work by simulation on the modelling of SFAP, MUAP, MUAPT and the sEMG signal. The most important result of this model is that signal processing tools can be applied to analyze and interpret real-world phenomena such as the effects of physiological , non physiological and sensing system parameters on the shape of the simulated sEMG signal.***

Keywords: detection system, fibres, modelling, motor unit , surface electromyography

1. INTRODUCTION

Surface electromyography (sEMG) is the study of muscle function through the electrical signals generated from it. It is used extensively to determine the muscle activation patterns of neuromuscular functions such as motor control, posture, and movement [1]. The sEMG signal depends on anatomical, physiological and detection system parameters [2]. sEMG signal simulation is important for interpreting the experimental recordings of the electromyogram [3] and is important for more understanding the muscle contraction from a point of view physiologic [4]. Many models for sEMG signal generation and detection were proposed in the past [5], [6], [7], [8] which were essentially distinguished by the volume conductor geometry (cylindrical, planar, or curvilinear), motor unit recruitment mechanism description, MU firing rate strategies.
When the action potential shape is the same in each point in the direction of propagation of the source, we aretalking here about a volume conductor invariant by space [2], [9], [10], however when the action potential shape is different from a point to another in the direction of propagation of the current source we are talking here about a volume conductor not invariant by space [3], [4], [11], [12].
From the mathematical point of view, analytical [9], [13] and numerical [14], [15], [16] methods were suggested for modelling the electrical properties of tissues separating the sources and the detection point. For the coordinate systems, cartesian [10], and cylindrical [17], [18] systems were used for the geometrical description of the volume conductor. The history of the different models recommended for the simulation of the volume conductor is summarized in table 1.
In the present study, the model of the volume conductor was described as in [17] and research findings of references [5], [6], [7], [8]. The modelling of the SFAP was mainly based on the model established in [17]. The MUAP, trains of MUAP, MUs recruitment, rates of fire strategies, distribution of diameters on motor units, distribution of conduction velocities over motor units, distribution of fibres inside motor units, distribution of motor units inside muscle, distribution of neuromuscular junctions in the motor endplate area, and distribution of right and left tendons in the extremities of the motor units were based on models described in references [5], [6], [7], [8].
It is known that the main purpose of models is to predict results whose experimental verification validates or negates the equations, hypothesis and assumptions used in the model. Despite its limitations, our model is able to help us interpret real phenomena.
Particularly, our developed model has proven its effectiveness in the analysis and interpretation of the effects of anatomical (layers thicknesses and the MUs depths), physiological (conductivities of the volume conductor layers) and the detection system (electrodes configuration, interelectrode distance and shape and size of electrodes) parameters on the shape of sEMG signal.
Our model also has the possibility of being used to produce several practical work brochures such as the modelling of the SFAP, the modelling of the MUAP and MUAPTs and finally the modelling of the sEMG signal. Other brochures can also be produced by applying signal processing tools to the simulated signals.

2. METHODS

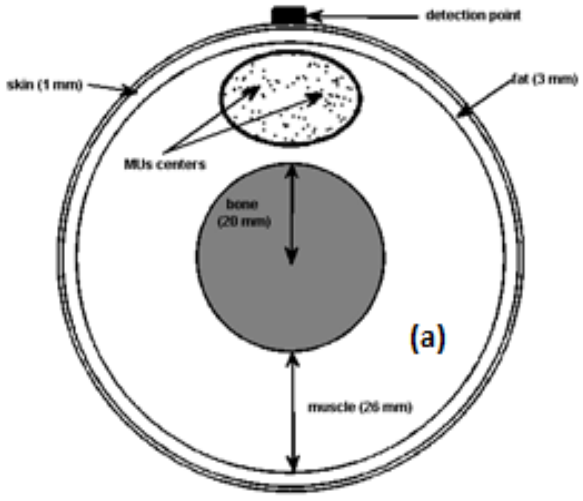
In this section, we described the different stages to simulate sEMG signal.

Table 1. Proposed volume conductor models.

Reference	Year	Volume conductor geometry	Homogeneity/non-homogeneity of the layers
Space invariant models			
[19]	1991	Cylindrical	Muscle and fat
[13]	1998	Planar	Muscle
[9]	1999	Planar	Muscle
[10]	1999	Planar	Muscle, fat and skin
[2]	2001	Planar	Muscle, fat and skin
[18]	2002	Cylindrical	Muscle, fat and skin
[17]	2004	Cylindrical	Bone, muscle, fat and skin
Non space invariant models			
[3]	2004	Planar	**Muscle and fat** The non-homogeneity of the muscle layer which is due to the different alignments of the fibres.
[11]	2005	Planar	**Muscle and fat** The non-homogeneity is due to the presence of circles in the subcutaneous layer.
[12]	2006	Planar	**Muscle and fat** The non-homogeneity is due to the variation of the conductivity along the direction of the fibres.
[4]	2006	Cylindrical for muscle Planar for fat	**Muscle and fat** The non-homogeneity of the muscle layer which is due to the triangular arrangement of the fibres in the muscle layer.
[20]	2008	Cylindrical for muscle Planar for fat	**Muscle, fat and skin** The non-homogeneity of the muscle layer which is due to the presence of an anatomical semi-cylindrical structure located in the muscle layer (case of superficial bone or blood vessel).

2.1. Surface EMG simulation

An sEMG signal generated in a pool of 120 motor units was simulated. The volume conductor model was described as in [17]. The recruitment of motor unit (MU) and the rate of fire strategies were described according to the reference **[5]**. All the parameters of the model were shown in the Table 1 of the reference [21].



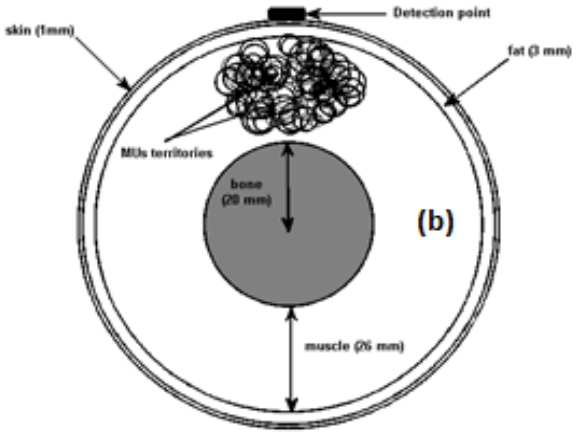


Figure 1. Cross-section of the multi-layered cylindrical volume conductor model. (a): In the muscle layer, an elliptical-shaped muscle is shown. Within this muscle the motor units centers are uniformly distributed. (b): the motor units territories are uniformly distributed inside the elliptical muscle [21].

2.1.1. MUAP simulation [21]

It is known that the MUAP is the sum of the action potentials generated from the fibres innerved by the same axon. In our model, the simulated muscle was described

as in **[8].** It contains 120 motor units (MUs) that are uniformly dispersed **[5], [8]** (see Fig. 1). The muscle fibres (MFs) scattering within MUs are well described in **[5], [8]** (see Fig. 2).

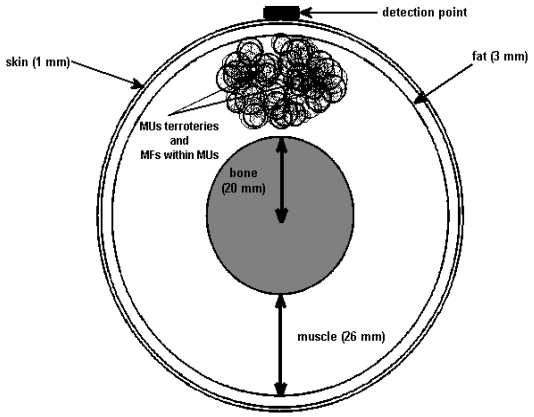


Figure 2. The territories of motor units which are uniformly distributed inside the elliptical muscle Thus, the muscle fibres axis are uniformly distributed inside each MU.

The scattering of the MUs diameters was done as described in **[6]** and **[7]**. According to the numerical details of our model (see table 2 in [21]) the alpha motoneuron of the samallest MU innerves 63 fibres, however, the alpha motoneuron of the the largest one innerves 1005 fibres (see Fig. 3 and table 2 of the reference [21] for more numerical details).

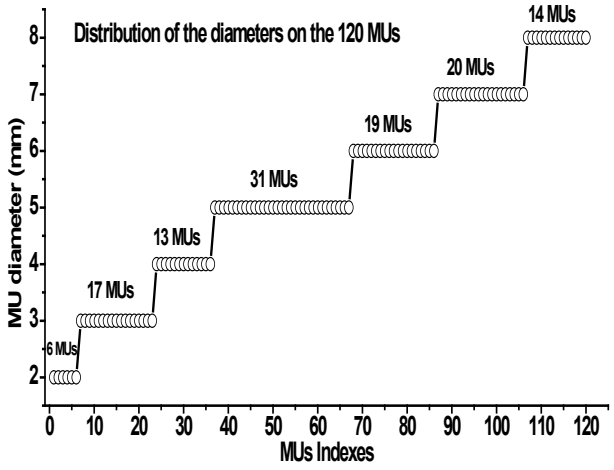


Figure 3. A group of motor units takes the same diameter.

The current density source which is proportienal to the second derivative of the intracellular action potential (IAP) is an important step in the SFAP simulation. Its (IAP) simulation was based on the analytical expression developped by Rosenfalck [13], **[22]**. Fig. 4 shows how the current density source generated at the neuromuscular junction, propagated along the fibre and extinguished at the tendons.

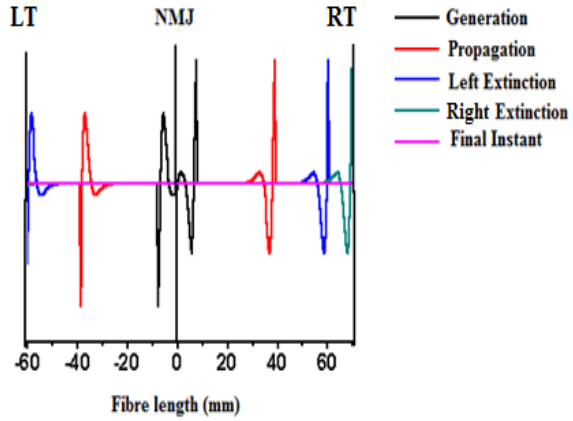


Figure 4. The current density source (its generation, its propagation and its extinction). LT: indicates left tendon and RT indicates right tendon [2], [17].

As a rule, large motor units have large fibres and higher conduction velocity than small MUs. The distribution of the conduction velocity on the recruited MUs was described in **[5]** (we simulated this in Fig. 5).

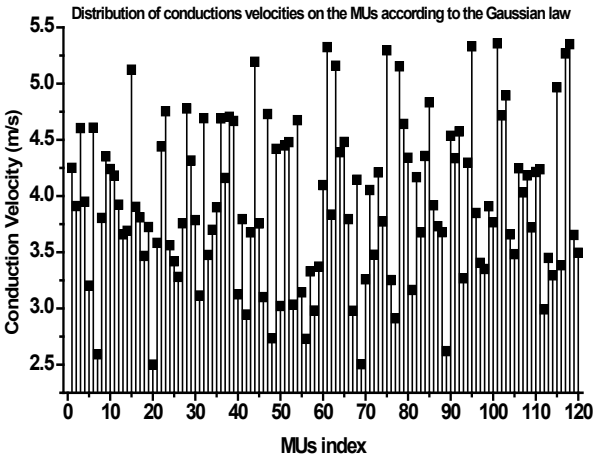


Figure 5. Conduction velocities were normaly distributed on the MUs.

The simulated sEMG signals were recorded by the seven spatial filters shown in Fig. 6. The electrodes location and shape, the interelectrode distances and the fibres inclination were described as in **[23]**.
The physiological and non-physiological parameters of the model and the numerical details of it are well shown and described in Table 1 and Table 2 of the reference [21].

2.1.2. Principle of motor unit recruitment [21]

The motor unit considers itself as a point of connection between the central nervous system and the muscle that produces the movement. The role of a motor neuron is to discharge action potentials and excite muscle fibers to contract [25].
Excitations of the motor unit recruitment thresholds of a muscle are modeled by the following relationship [5]:

$$RTE(i) = e^{\left(\frac{\ln RR}{n}\right)i} \quad (1)$$

Where i is the MU index,

ln indicates the natural logarithm, RR is the maximum value that can be reached by the maximum voluntary contraction.
n is the number of recruited MUs.

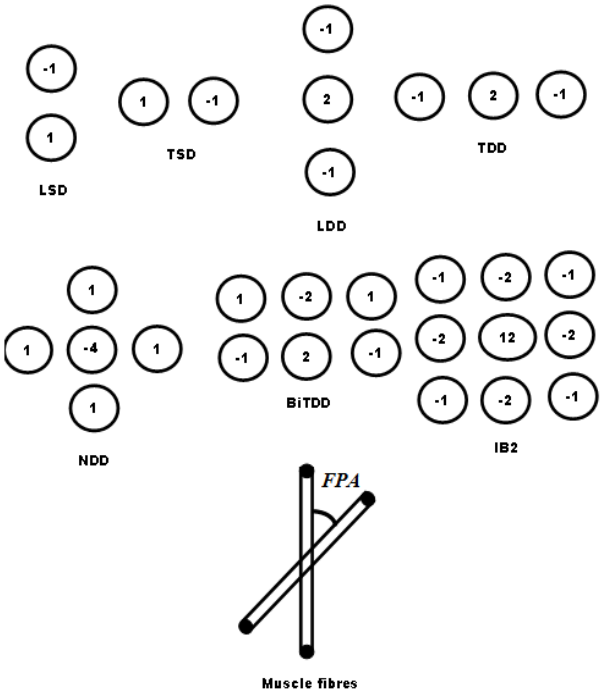


Figure 6. Electrodes configuration relative to the muscle fibers direction [23], [24].

A narrow and a braod recruitment ranges (RRs) were distinguished. The value of the narrow recruitment range was set at 30%) and the value of the braod recruitment range was set at 70%. A motor unit remains inactive as long as the excitation force is below to its recruitment threshold [5].

2.1.3. Strategies of discharge rate [21]

The MUAPT is created after a pseudo periodique discharge of the motor unit axone [6].
According to [5], the repeated discharge of motor units has four characteristics:
A minimum discharge frequency.
A relationship between excitation and motor unit discharge frequencies.
Maximum discharge frequency.
A variability of inter-pulse intervals under steady-state excitation.
If the MU recruitment condition is satisfactory, each MU begins to discharge with a minimum discharge frequency (MFR) which is the same for all recruited MUs and is equal to 8 Hz.
The excitatory drive and the firing rate are linked by the expression (2) in [21], however, the peak firing rate and the recruitment threshold are linearly related by the expression (3) in [21].

Two types of discharge frequency strategies were distinguished [5].
The first strategy (FR1) models the phenomenon called onion-skin of MU discharge frequencies observed from voluntary contractions. In this strategy, the slope of the relationship between excitation and motor unit discharge frequencies is the same for all MUs [5]. Fig. 7a shows the variation in MU discharge frequencies as a function of excitation according to the FR1 strategy, when voluntary muscle contraction is equal to 100% (Fig. 7a) of maximum excitement. In this strategy, the firing frequencies of all MUs have the same slope and the initial recruited MU takes the largest PFR and the latest recruited MU takes the smallest PFR.
The second strategy (FR2) models the reverse onion-skin phenomenon. In this strategy, the slope of the relationship between excitation and MUs discharge frequencies is the same as in the case of the FR1 strategy. However, in this strategy, MUs with high recruitment thresholds take the highest discharge frequencies and MUs with low recruitment thresholds take the lowest discharge frequencies (Fig. 7.b) [5], [26], [27], [28].

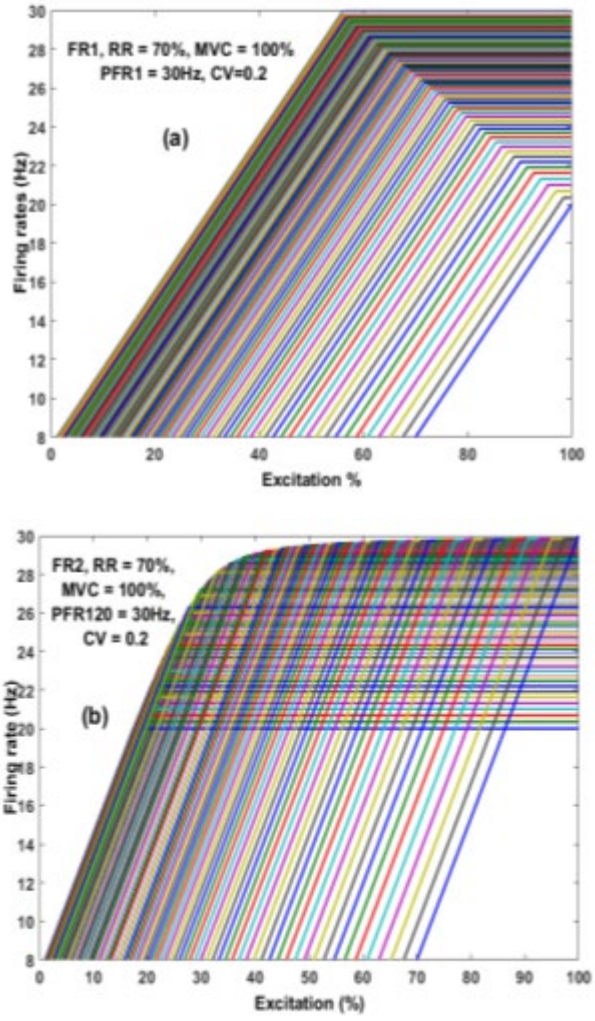


Figure 7. Firing rates satrategies: (a) onion skin (FR1) and (b) reverse onion skin (FR2). MVC: Muscular Voluntary Contraction. RR: Recruitment threshold. PFR: Peak Firing Rate. CV: Constant of variation [21].

The inter-pulse intervals (ISIs) of MU discharge are modeled according to the Gaussian law [5]. Figure 8 shows the discharge times of the recruited MUs. Note that for the same MUAP train, the duration between successive pairs of load instants is not the same. This is due to the Gaussian distribution of the ISIs. We also notice that all the MUs do not begin to discharge at the same time (there is an instant lag between a recruited motor unit and the unit that follows it).

3. RESULTS

Fig. 9 shows MUAPs generated from two MUs with different locations inside the muscle and recorded with the LSD fiter. The shape of the MUAP is strongly linked to the coordinates and diameter of the MU.

Fig. 10 shows examples of MUAP trains signals generated in two MUs with different coordinates inside the muscle and detected by the LSD system. The difference between this figure and Fig. 9 lies in the MUAP train (MUAPT) which replaces the MUAP. The MUAPT is created according to the MU recruitment mechanism and the MU firing rates strategies.

In addition to what was shown in Fig. 10, the figure. 11 also shows the location of the two MUs in the muscle such that they are distinguished by their positions, their dimensions and the number of fibres innervated by them.

Fig. 12 shows MUAP trains generated by twelve recruited MUs in steps of 10 among the 120 MUs and detected by the LSD system. It should be noted that each pulse (firing time) in Fig. 8 corresponds to a MUAP in Fig. 12.

The point-by-point sum of the 120 MUAP trains of which only 10 are represented in Figure 12 gives the total EMG signal shown in Figure 13. This figure shows the resultant sEMG signals generated in a pool of 120 MUs and detected by the systems shown in Fig. 6. All simulation parameters are the same, except the electrode configuration which makes the difference between the shape and amplitude of the simulated sEMG signals.

4. THIS MODEL IS THE PLATFORM OF OUR PREVIOUSLY PUBLISHED WORKS

In [30], to estimate the relation beteween the MVC level and the misealignement of the fibres, we computed the cross-correlation coefficient (CC) of sEMG signals recorded from muscle of parallel fibres and those recorded from muscle with inclined fibres. To reach this goal, we used a database of sEMG signals generated by the model developed in [21]. Our results showed that the correlation coefficient decreased when the angle of inclination increased.

The purpose developped in [21] was to assess the influence of the electrodes shape and size and interelectrode distance on sEMG signals Gaussianity and linearity levels when the MVC level varies from 10% to 100%. The effects of other parameters were also examined [21]. The kurtosis was used as a factor to measure these levels. We mainly revealed that high Gaussianity and linearity levels were obtained with the LSD configuration.

The objective in [31] was to categorize the most known spatial fiters allowing to their selectivity in all directions. The work was articulated by synthetic electromyographic signals produced in an elliptical-shaped muscle [21]. In order to estimate the level of isotropy of each filter, the mean power (MP) of the signals recorded in the case of parallel and inclined fibres was computed. In such a study, we showed that the sensitivity of the systems to the fibres inclination was less affected by the change of the distance between the detection point and the sources than by the change of the electrodes shape and dimensions.

The main aim of our previous work [32] was to estimate the muscle fatigue by computing the mean absolute value (*MAV*) and the median frequency (*MDF*) in function of the muscular voluntary contraction in the case of three values of the maximum frequency and interelectrode distance. We showed that an increase of the level of MVC implies an increase in the MAV of EMG signals and a decrese in the MDF.

The main purpose in [33] was to guesstimate the degree of normality of sEMG signals recorded from an elliptical-shaped composed of 120 MUs [21] in function of the fibres misealignement. For that, the Kurtosis of sEMG signals detected when the fibres are parallel with respect to the electrodes arrangment and those detected when the fibres are inclined was computed and used as a parameter of estimation. The main result of such a study was that the MKF filter detect is more Gaussian with most inclination angles compared to the other systems.

The study of the reference [23] aimed to evaluate the influence of three parameters related to the detection system on correlation coefficient between MUAPs detected from MU when their fibres are parallel and MUAPs recorded from MU composed of misealignement fibres. In [23], we showed that the effects of the studied sensing system parameters on the coefficien of correlation between parallel and inclined fibres is strongly linked to the used spatial filter. For each studied parameter, the sEMG signals detected by the inverse binomial of order two (IB2) filter are the most correlated and those recorded by the MKF system are the least interconnected. Therefore, IB2 system is suggested for detecting sEMG signals generated from inclined fibers.

Our last work [24] aimed to study the capacity of electrodes configuration to discriminate between adjacent MUAPs when the fibres are inclined. This subject falls within the framework of evaluating the sensitivity of filters for sEMG signal recording. Our results showed that the MU position and dimension and also fibres misealignment have a great influence on the aptitude of a detection system to differentiate two MUAPs. In general, we have shown that for a given interval of inclination angle, the bi-transversal double differential (BITDD) fiter is best placed to distinguish between two MUAPs.

Therefore, with the development of this model, we have taken a big step towards its exploitation to develop other results.

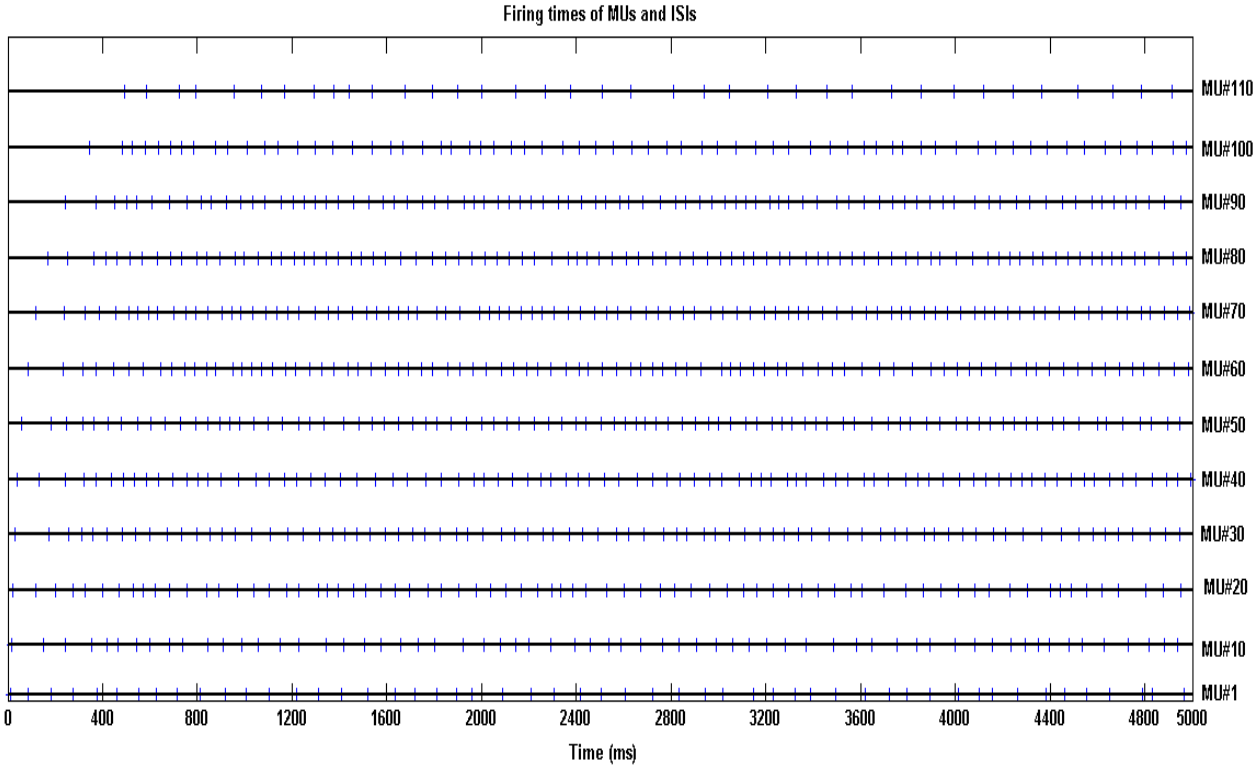


Figure 8. Firing times of MUs and the interspike intervals. Each bar corresponds to a motor unit action potential.

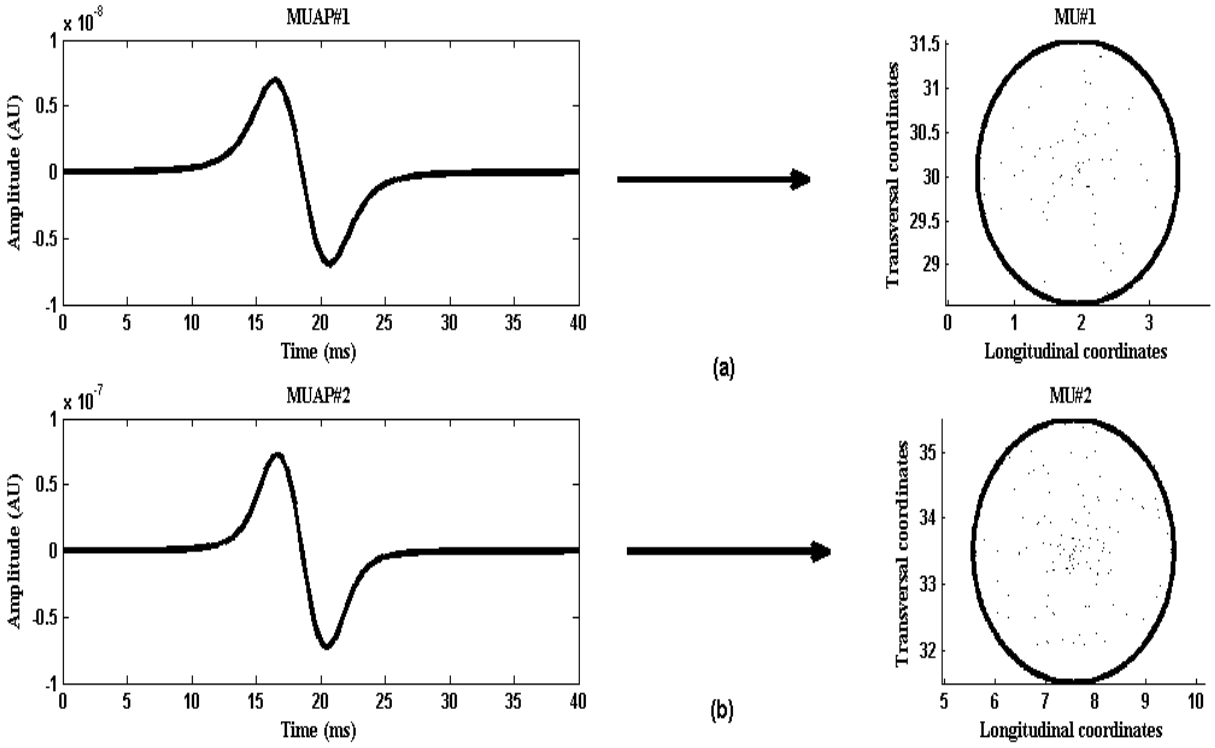


Figure 9. Example of simulated MUAPs (left side) generated from two MUs (right side). The coordiantes of the two MUs are shwn on the right of the figure. The fibres were uniformly distributed inside the two MUs. The number of MFs with each MU is linked to its size.

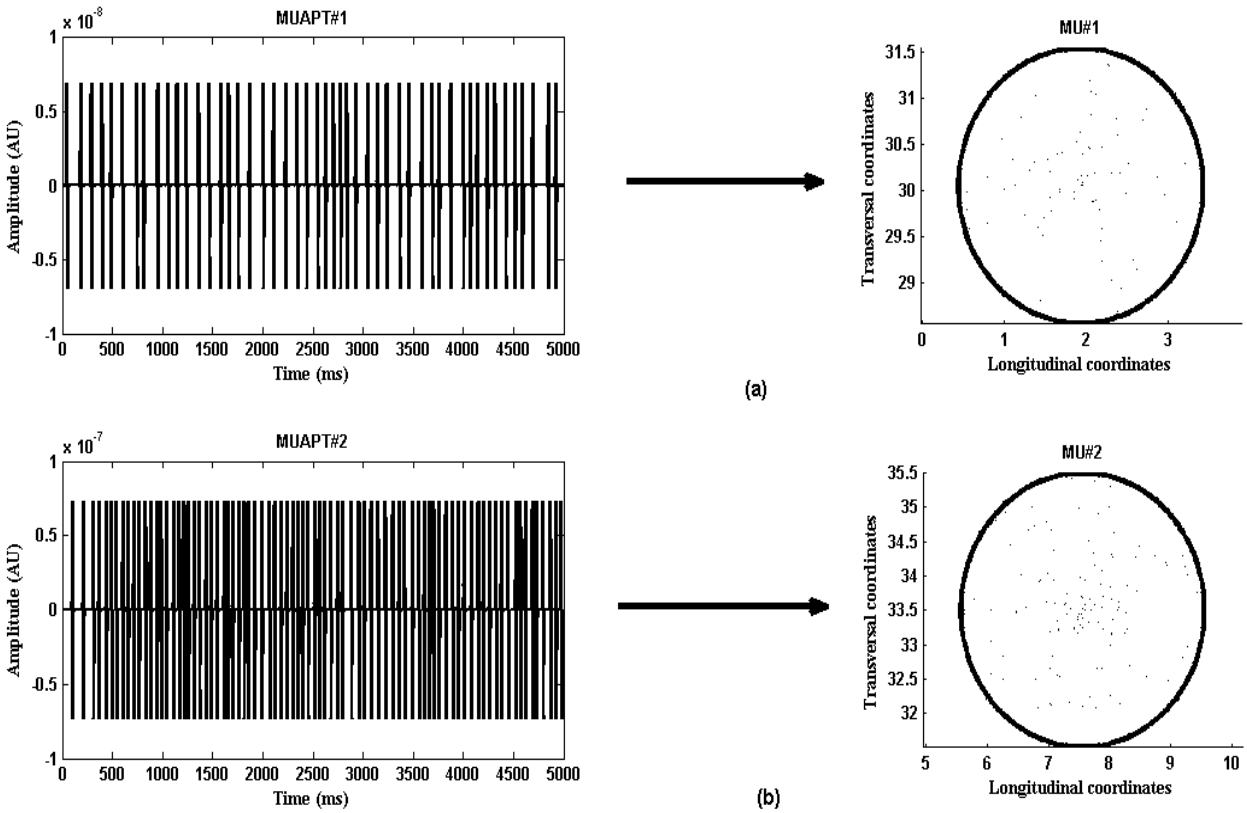


Figure 10. Examples of simulated MUAPTs (left side) generated from two MUs (right side) and recorded by the LSD system. The coordiantes of the two MUs are shwn on the right of the figure.

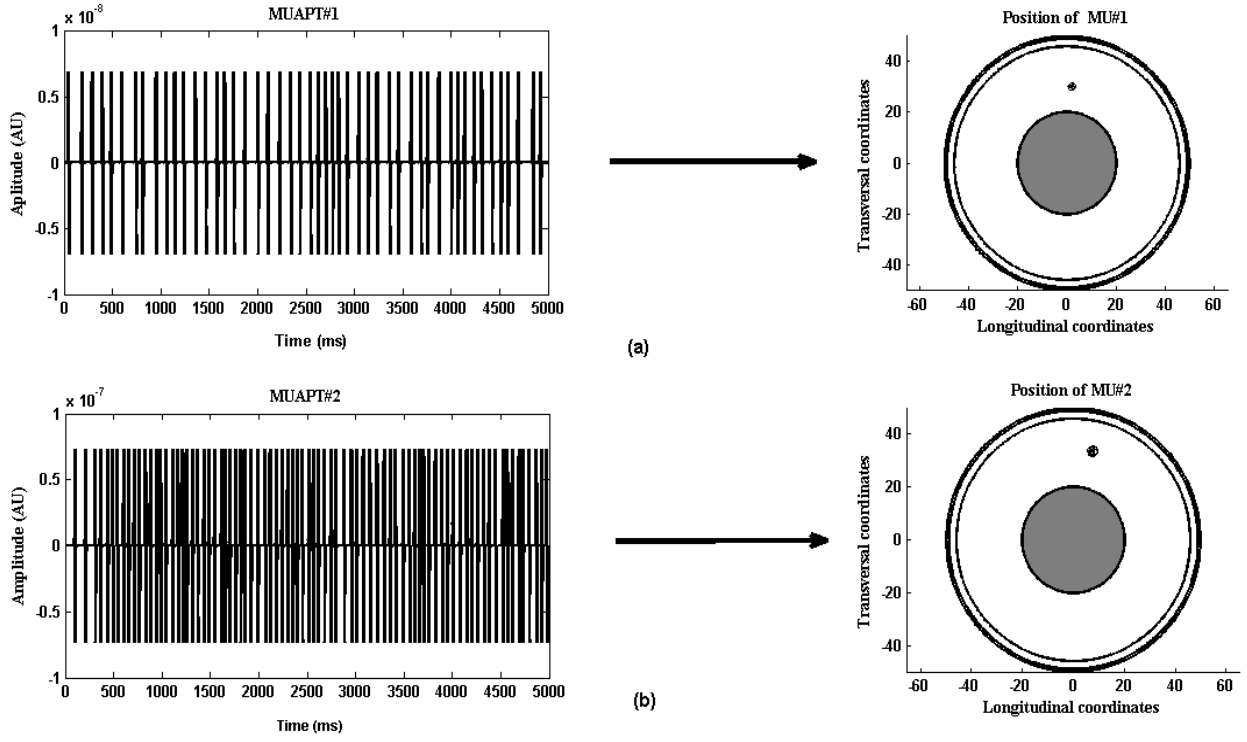


Figure 11. The left side of this figure is the same as the lefet side of Fig. 10, the difference resides only in the right side where we showed the coordinates of the two MUs indoors the muscle.

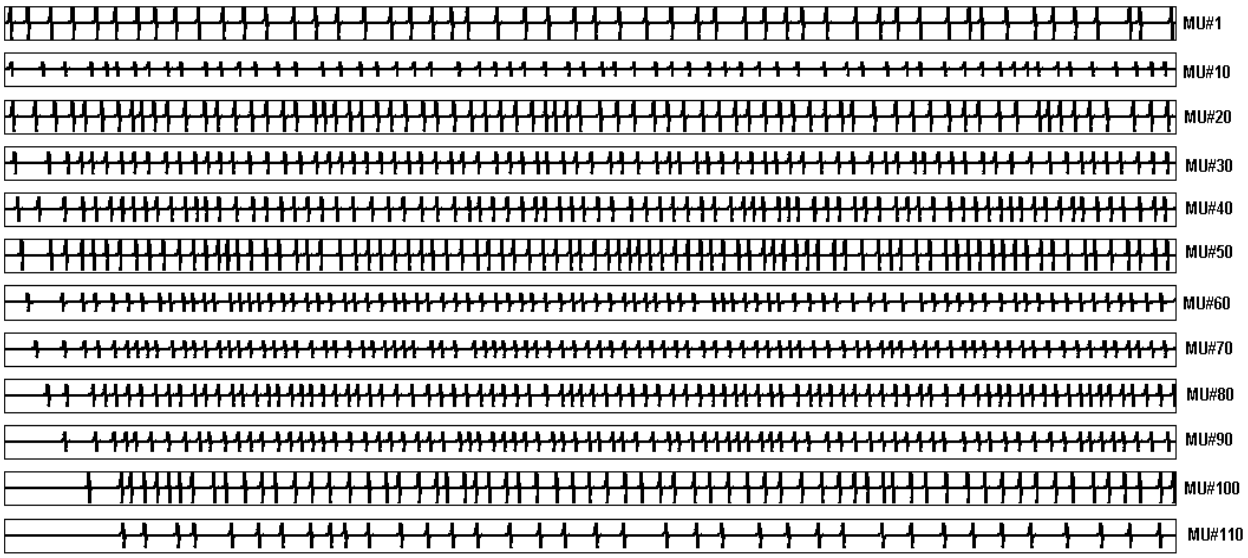
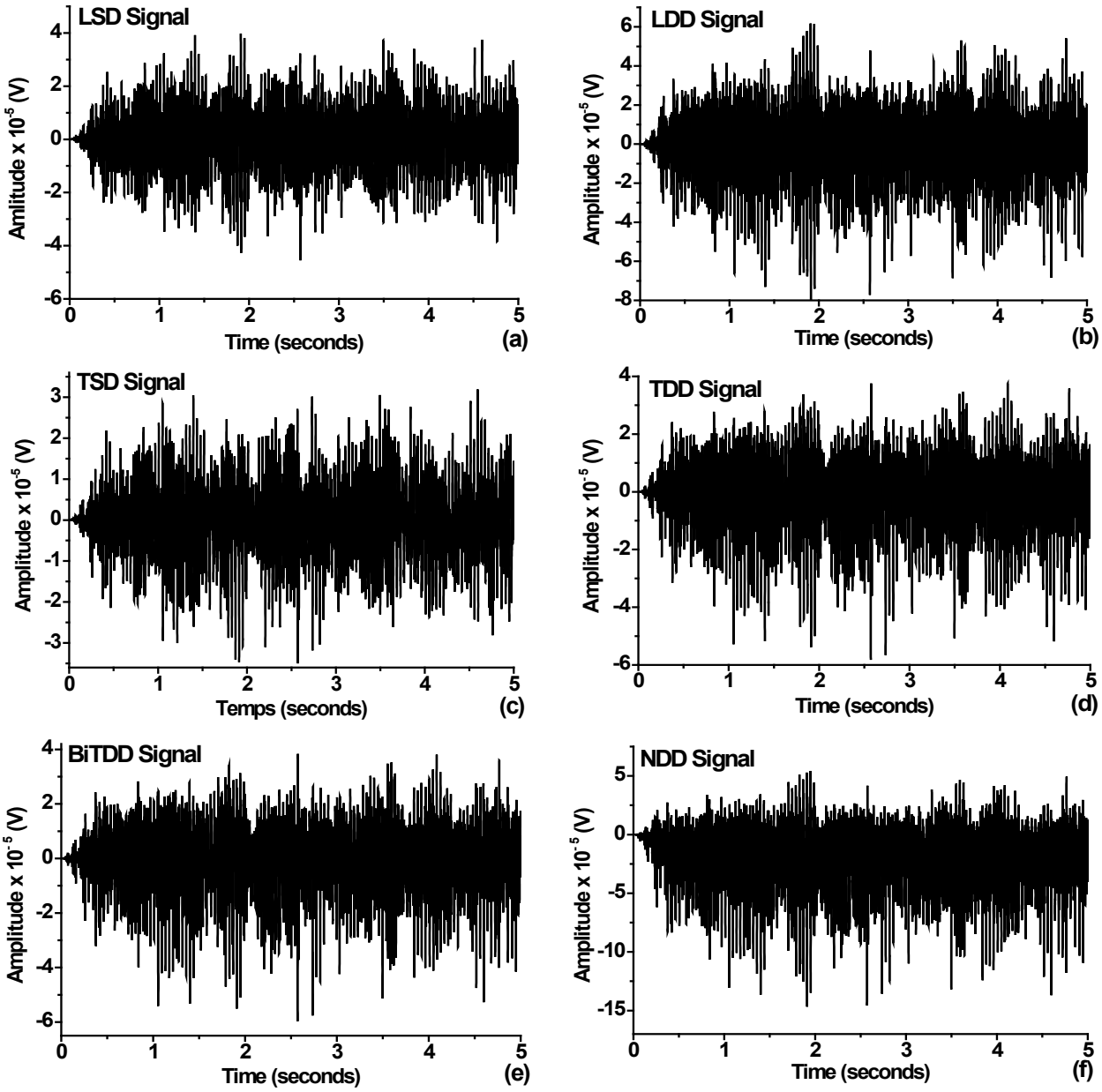


Figure 12. The trains of the MUAPs.



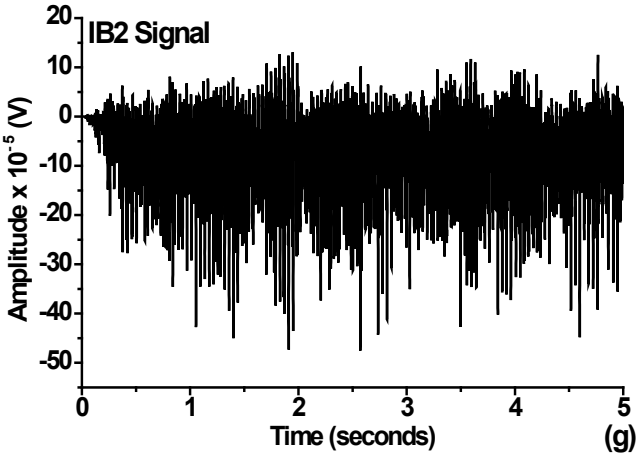


Figure 13. The resultant sEMG signals.

The development of this model in 2015 [29] encouraged us to publish other results based on it [21], [23], [24], [30], [31], [32], [33].

5. DISCUSSION

The model we have developed is a combination of models previously proposed [2], [5], [6], [7], [8], [17]. For the modeling of SFAP, we based on the two models developped in [2] and [17] and for the distribution of the diameters on the set of MUs, we founded our study on the model proposed in [7]. We used the results of the works [5], [6], [8] for the description of motor unit recruitment mechanism, motor unit firing rates strategies, distribution of muscle fibre lengths, distribution of MUs, distribution of conduction velocities on motor units, distribution of muscle fibres within motor units, distribution of neuromuscular junctions in motor endplates and the distribution of right and left tendons of muscle fibres innervated by the same axone. The exploitation of the previous models proposed allowed us to avoid the shortcomings of each of them. Indeed, each new model takes into consideration the insufficiencies of the previous model and so on. For the SFAP generation and detection, we used the models that had a great influence on the shape of the simulated EMG signal [2] and [17]. Specifically, a good modelling of the SFAP implies a worthy simulation of the EMG signal since the shape of this last takes the form of the SFAP according to the electrodes configuration.

In addition to these combinations, we added some new details. These details are mainly linked to the geometry of the muscle, the geometry of the motor units and the distribution of muscle fibres in the motor units. In addition, we can also determine the number of MUs with any diameter (see Fig.3 and Table 2 of the reference [21]), to the conduction velocity corresponds to each motor unit (see Fig. 5), to the number of fibres belongs to the sameMU and their coordinates (see Table 2 of the reference [21] and Fig. 9), to the geometry of the motor unit territories in the muscle area (see Fig. 1b), to the MUAPs and the MUAPTs and the corresponding motor unit (see Fig. 9 and Fig. 11).

We can also determine the coordinates of each recruited motor unit and the corresponding MUAP.

Although simulation models have limited practical interests [34], [35], we see that in the case of absence of equipment at the laboratory level to carry out practical work, the importance of simulation models has emerged for understanding the real phenomena. For this reason, we thought of developing this model to precess the sEMG biomedical signal.

However, our model suffers from slow execution time. The main cause of this long time was due to the large number of MFs in the muscle area. For example, to generate a single EMG signal with a density of fibres in the muscle area of 20 fibres/mm^2 and with a PC having the following properties: Intel(R) Core (TM) 2 Duo CPU P7350 @ 2.00GHz (2CPUs), ~2.0GHz RAM 3GB, runtime exceeds four hours. To minimize this execution time, a computing station with advanced properties is required.

6. CONCLUSIONS

The sEMG signal generation and detection model that we have developed is considered as a basic model in the field of electromyography.

This model can be consulted by researchers in this field to exploit it in other applications (sorting of sEMG signals, evaluation of the effects of the volume conductor and detection system parameters).

In addition, despite its limitations (signals simulated and not realy recorded), our model remains useful especially for didactic applications (This model helps researchers understand how the sEMG signal is generated and detected).

Moreover, our model can be considered as a source of simulated sEMG signals such that an unlimited number of sEMG signals can be generated by changing physiological and non physiological parameters. Its usefulness has clearly appeared in problems that use

artificial intelligence methods since these methods require a large database and our model can meet this requirement.

7. REFERENCES

[1] Östlund N. Yu J. Roeleveld K. Karlsson JS. Adaptive spatial filtering of multichannel surface electromyogram signals. Med. Biol. Eng. Comput 2004; 42(6): 825-831.

[2] Farina D. Merletti R. A novel approach for precise simulation of the EMG signal detected by surface electrodes. IEEE. Trans. Biomed. Eng 2001; 48 (6): 637-646.

[3] Mesin L. Farina D. Simulation of surface EMG signals generated by muscle tissues with inhomogeneity due to fiber pinnation. IEEE. Trans. Biomed. Eng 2004; 51 (9): 1521-1529.

[4] Mesin L. Simulation of surface EMG signals for a multi-layer volume conductor with triangular model of the muscle tissue. IEEE. Trans. Biomed. Eng 2006; 53(11): 2177-2184.

[5] Fuglevand AJ. Winter DA. Patla AE. Models of recruitment and rate coding organization in motor-unit pools. J. Neurophysiol 1993; 70 (6): 2470-2488.

[6] Stashuk DW. Simulation of electromyographic signals. J. Electromyogra. Kinesiol 1993 3 (3): 157-173.

[7] Wang W. Stefano Ade. Allen R. A simulation model of the surface EMG signal for analysis of muscle activity during the gait cycle. Comput. Biol. Med 2006; 36 (6): 601-618.

[8] Keenan KG. Farina D. Meyer FG. Merletti R. Enoka RM. Sensitivity of the cross-correlation between simulated surface EMGs for two muscles to detect motor unit synchronization. J. Appl. Physiol 2007 102 (3): 1193-1201.

[9] Merletti R. Lo Conte L. Avignone E. Guglielminotti P. Modelling of surface myoelectric signals – part I: model implementation. IEEE. Trans. Biomed. Eng 1999; 46 (7): 810-820.

[10] Farina D. Alberto R. Compensation of the effect of sub-cutaneous tissue layers on surface EMG : a simulation study. Med. Eng. Physics 1999; 21 (6-7): 487-497.

[11] Mesin L. Farina F. A model for surface EMG generation in volume conductors with spherical inhomogeneties. IEEE. Trans. Biomed. Eng 2005; 52 (12): 1984-1993.

[12] Mesin L. Farina D. An analytical model for surface EMG generation in volume conductors with smooth conductivity variations. IEEE. Trans. Biomed. Eng 2006; 53 (5): 773-779.

[13] Dimitrov GV. Dimitrova N.A. Precise and fast calculation of the motor unit potentials detected by a point and rectangular plate electrode. Med. Eng. Phys 1998; 20 (5): 374-381.

[14] Farina D. Mesin L. Martina S. Advances in surface EMG signal simulation with analytical and numerical descriptions of the volume conductor. Med. Biol. Eng. Comput 2004; 42 (4): 467-476.

[15] Lowery MM. Stoykov NS. Taflove A. Kuiken TA. A multiple-layer finite-element model of the surface EMG signal, IEEE. Trans. Biomed. Eng 2002; 49 (5): 446-454.

[16] Mesin L. Joubert M. Hanekom T. Merletti R. Farina D. A Finite Element Model for Describing the Effect of Muscle Shortening on Surface EMG. IEEE. Trans. Biomed. Eng 2005; 53 (4): 593-600.

[17] Farina D. Mesin L. Martina S. Merletti R. A surface EMG generation model with multilayer cylindrical description of the volume conductor. IEEE. Trans. Biomed. Eng 2004; 51 (3): 415-426.

[18] Blok JH. Stegeman DF. Van Oosterom A. Three-layer volume conductor model and software package for applications in surface electromyography. Ann. Biomed. Eng 2002; 30 (4): 566-577.

[19] Gootzen TH. Stegeman DF. Van Oosterom A. Finite limb dimensions and finite muscle length in a model for the generation of electromyographic signals, Electroencephalogr. Clin. Neurophysiol 1991; 81 (2): 152-162.

[20] Mesin L. Simulation of surface EMG signals for a multilayer volume conductor with a superficial bone or blood vessel, IEEE. Trans. Biomed. Eng 2008; 55 (6): 1647-1657.

[21] Messaoudi N. Bekka RE. Philippe R. Harba R. Assessment of the non-Gaussianity and non-linearity levels of simulated sEMG signals on stationary segments, J. Electromyogr. Kinesiol 2017; 32 (Feb): 70-82.

[22] Rosenfalck P. Intra and extracellular fields of active nerve and muscle fibres: A physico-mathematical analysis of different models. Acta. Physiol. Scand 1969; 321: 1-168.

[23] Messaoudi N. Bekka RE. Belkacem S. Effects of detection system parameters on cross-correlations between MUAPs generated from parallel and inclined muscle fibers. Polish. J. Med. Phys. Eng 2021; 27 (1): 87-97.

[24] Messaoudi N. Belkacem S. Bekka RE. Ability of spatial filters to distinguish between two MUAPs generated from MUs with different locations, sizes and fibers pennation. J. Instrument, 2023; 18 (3): P03041.

[25] Enoka RM. Motor Unit. Wiley Encyclopedia of Biomedical Engineering, 2006.

[26] Hu X. Rymer WZ. Suresh N. Motor unit firing rate patterns during voluntary muscle force generation: a simulation study. J. Neural. Eng 2014; 11 (2): 026015.

[27] De Luca CJ. Hostage EC. Relationship between firing rate and recruitment threshold of motoneurons in voluntary isometric contractions. J. Neurophysiol 2010; 104 (2) 1034-1046.

[28] Hu X. Rymer WZ. Suresh NL. Motor unit pool organization examined via spike-triggered averaging of the surface Electromyogram. J. Neurophysiol 2013; 110 (5): 1205-1220.

[29] Messaoudi N. Bekka R.E. (2015). From Single Fiber Action Potential to Surface Electromyographic Signal: A Simulation Study. In: Ortuño, F., Rojas, I. (eds) Bioinformatics and Biomedical Engineering. IWBBIO 2015. Lecture Notes in Computer Science, vol 9043. Springer, Cham. https://doi.org/10.1007/978-3-319-16483-0_32.

[30] Messaoudi N. Bekka RE. Belkacem S. Cross-Correlation Coefficient as a Means for Estimating the Effect of MVC level According to the Fibres Inclination. The Fifth International Conference on Electrical Engineering, ICEE2017, Boumerdes, Algeria, Proceedings, IEEE Xplore (2017b).

[31] Messaoudi N. Bekka RE. Belkacem S. Classification of the systems used in surface electromyographic signals detection according to the degree of isotropy. Adv. Biomed. Eng 2018; 7 (1): 107-116.

[32] Belkacem S. Bekka RE. Messaoudi N. Influence of MVC on Temporal and Spectral Features of Simulated Surface Electromyographic Signals. Critical. Reviews. Biomed. Eng 2019; 47 (5): 409-418.

[33] Messaoudi N. Bekka RE. Belkacem S. Influence of Fibers Inclination on the Degree of Gaussianity of Simulated Surface EMG Signals. ICBBT 2020, May 22–24, 2020, Xi'an, China.

[34] Merletti R. Temporiti F. Gatti R. Gupta S. Sandrini G. Serrao M. Translation of surface electromyography to clinical and motor rehabilitation applications: The need for new clinical figures. Translatio. Neurosci 2023; 14 (1): 1 20220279.

[35] Campanini I. Merlo A. Disselhorst-Klug C. Mesin L. Muceli S. Merletti R. Fundamental Concepts of Bipolar and High-Density Surface EMG Understanding and Teaching for Clinical, Occupational, and Sport Applications: Origin, Detection, and Main Errors. Sensors 2022; 22 (11) 4150.